Large-scale Monte Carlo simulations for the depinning transition in Ising-type lattice models

Lisha Si[a], Xiaoyun Liao[a], Nengji Zhou[a,*]

[a] *Department of Physics, Hangzhou Normal University, Hangzhou 310046, China*

Abstract

With the developed "extended Monte Calro" (EMC) algorithm, we have studied the depinning transition in Ising-type lattice models by extensive numerical simulations, taking the random-field Ising model with a driving field and the driven bond-diluted Ising model as examples. In comparison with the usual Monte Carlo method, the EMC algorithm exhibits greater efficiency of the simulations. Based on the short-time dynamic scaling form, both the transition field and critical exponents of the depinning transition are determined accurately via the large-scale simulations with the lattice size up to $L = 8\ 912$, significantly refining the results in earlier literature. In the strong-disorder regime, a new universality class of the Ising-type lattice model is unveiled with the exponents $\beta = 0.304(5), \nu = 1.32(3), z = 1.12(1)$, and $\zeta = 0.90(1)$, quite different from that of the Edwards-Wilkinson equation.

Keywords: `Dynamic critical phenomena, Monte Carlo methods, Depinning transition, Domain-wall dynamics`

1. Introduction

Driven by a constant force in the presence of the quenched disorder, the interface moves with a steady-state velocity, while it is pinning when the force is weak compared to the random noise. Between them, there exists a second-order dynamical phase transition, called as the "*depinning transition*" [1, 2, 3, 4, 5, 6, 7, 8]. For several decades, the depinining transition has been the focus of the experimental and theoretical research, which are common to a wide variety of phenomena, including the liquid invasion in porous media [9], the contact line in wetting [10], the vortices in type-II superconductors [11, 12], the charge-density waves [13], the fracture propagation [14, 15], the dislocation dynamics in crystal plasticity [16], and the domain-wall motions in ferromagnetic and ferroelectric materials [17, 18, 19, 20]. Practically, understanding the fundamental mechanism of the depinning transition plays an important role in

*Corresponding author
Email address: `zhounengji@hznu.edu.cn` (Nengji Zhou)

predicting and controlling the motions of the magnetic domain walls in nanomaterials [21, 22, 23], thin films [8, 24], and semiconductors [20, 25], which is key to the realization of the new classes of potential nonvolatile storage-class devices [26, 27].

Theoretical approaches to the domain-wall dynamics are typically based on the phenomenological models, such as the Edwards-Wilkinson equation with quenched disorder (QEW) and its variants [28, 29, 30, 31]. With these equations, the domain wall in a two-dimensional system can be effectively described by a single-valued elastic string, and the static and dynamic critical exponents of the depinning transition, i.e., β, ν, z, and ζ, are measured numerically, though the discrepancies are still large in the literature [32, 33, 34, 35]. For example, it reaches nearly 30 percent in the velocity exponent β. Recently, extensive simulations of the QEW at the depining transition have been performed with a lattice size up to $L = 8\ 192$ [28]. Based on the short-time dynamics method, the universality class of the depining transition is identified with the exponents $\beta = 0.245(6), z = 1.433(7), \zeta = 1.250(5)$, and $\nu = 1.333(7)$, which are robust under the changes of the disorder realization including the random-bond and random-field characters. Moreover, the scaling relation $\beta = \nu(z - \zeta)$ is revealed, consistent with the prediction of the functional renormalization group theory [36, 37]. However, most experiments reported that the roughness exponent is $\zeta \approx 0.6 - 0.9$ [1, 15, 31, 38, 39], smaller than that of the QEW equation, suggesting that detailed microscopic structures and interactions of real materials should be concerned.

Besides, the dynamical behaviors of the domain walls in ferromagnetic nanowires are also investigated via the micromagnetic simulations with the Landau-Lifshitz-Gilbert (LLG) equation depicting the time evolution of the orientation of the magnetization distribution, $m(\vec{r}, t)$ [40, 41, 42]. However, the LLG equation is too complicated to be simulated for the depinning transitions in ultrathin ferromagnetic or ferroelectric films. The Ising-type lattice models are then introduced with much simpler microscopic structures and interactions [43, 44, 45, 46]. In this paper, we use the random-field Ising model with a driving field (DRFIM) and the driven bond-diluted Ising model (DBDIM) as examples. For a long time, it has been invariably stated that the QEW equation and DRFIM model belong to the same universality class [43, 46, 47]. However, significant deviations of the critical exponents have been reported in recent works [48, 49], which could not be ruled out by statistical errors. It was argued that the difference may be induced by the intrinsic anomalous scaling and spatial multiscaling of the DRFIM at the depinning transition. Unfortunately, a weak dependence of the critical exponents on the strengthes of the random fields is found in the disorder regime $\Delta \in [0.8, 2.3]$ [50]. Hence, it remains ambiguous that the depinning transition of the DRFIM belongs to a new dynamic universality class or it only has a correction to the universality class of the QEW equation due to the influence of the first-order phase transition occurring at $\Delta \leq 1$. To solve this issue, we will identify the critical exponents of DRFIM in the regime of the strong disorder $\Delta \gg 1$ in this article.

Early studies of the depinning transition were always focused on the steady-

state velocity $v(L)$ of the domain wall [4, 35, 43, 51]. Suffering from severe critical slowing down, however, it is quite arduous to obtain the exact transition field H_c and critical exponents. Adopting the short-time scaling form [52, 53], both the static and dynamic exponents β, ν, ζ, and z can be easily and accurately determined from the nonsteady relaxation of the domain interface since the spatial correlation length is short [28, 33, 48]. Due to the limitation of the computing resources, however, the system size and simulation time are insufficient in previous work for the depinning transition in the DRFIM, which are up to $L = 1\ 024$ and $t_{max} = 2\ 000$ [48, 50], much smaller than those in the QEW equation, $L = 8\ 192$ and $t_{max} = 8\ 000$ [28]. It may result in a systematic error in the determination of the critical driving field H_c. Accordingly, larger spatial and temporal scales are needed in the simulations to obtain more precise results for the depining transition in the DRFIM.

In this paper, an optimized Monte Carlo method is developed, termed as the "extended Monte Calro" (EMC) algorithm. Adopting the EMC, much smaller time of the Central Processing Unit (CPU) is taken for the depinning transition, in comparison with that of the usual Monte Carlo method. By extensive simulations, the transition point and critical exponents of the DRFIM are then accurately determined for various strengthes of the quenched disorder, and a new universality class is unveiled. In addition, the depinning transition in another Ising-type lattice model, DBDIM, is also investigated for comparison. In Sec. 2, the models, EMC algorithm, and scaling analysis are described, and in Sec. 3, the numerical results are presented. Finally, Sec. 4 includes the conclusion.

2. Methodology

2.1. Model

The DRFIM is one of the simplest demonstration to study the depinning transition in the disorder media with microscopic structures and interactions. The Hamiltonian of the DRFIM can be written as

$$\mathcal{H} = -J \sum_{<ij>} S_i S_j - H \sum_i S_i - \sum_i h_i S_i, \tag{1}$$

where $S_i = \pm 1$ is the classical Ising spin of the two-dimensional rectangle lattice with $2L \times L$, the random field h_i is uniformly distributed within an interval $[-\Delta, \Delta]$, and H is a homogeneous driving field. The initial state that spins are positive in the sublattice on the left side and negative on the right side, is used to build a perfect domain wall, also referred to as a "domain interface", in the y direction. The direction perpendicular to the domain interface is then set to the x axis. Antiperiodic and periodic boundary conditions are used in x and y directions, respectively. To eliminate the pinning effect irrelevant for disorder, we rotate the square lattice such that the initial domain wall orients in the (11) direction of the square lattice, as shown in Refs. [43, 48, 51, 54].

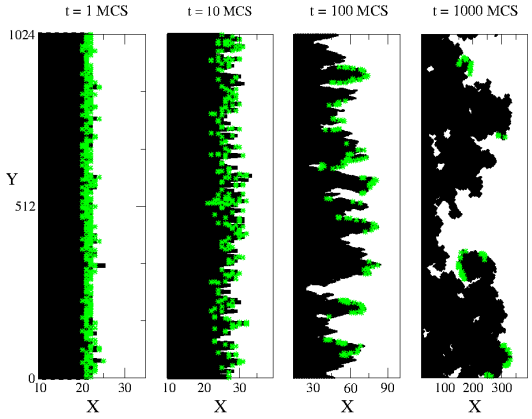

Figure 1: Time evolution of the spin configuration under the uniform distribution of the random fields. The black and white correspond to the spin up ($S_i = 1$) and down ($S_i = -1$), respectively, and the stars denote the activated spins within the domain interface. As the time t grows, overhangs and islands are created.

After preparing the initial state, a usual Monte Carlo method is adopted with standard one-spin flips in the simulations. Simply speaking, we update each spin with the following procedure. Firstly, we randomly choose a single spin S_i in the two-dimensional lattice. The change of the total energy is then calculated after we flip the spin $S_i \to S_i'$,

$$\begin{aligned} \delta E &= \mathcal{H}(S_i) - \mathcal{H}(S_i') \\ &= (S_i' - S_i)\left[-J\sum_j S_j - H - h_i\right]. \end{aligned} \tag{2}$$

Only when $\delta E < 0$, the flip is accepted, otherwise the spin state S_i remains. A Monte Carlo time step (MCS) is defined by $2L^2$ single-spin updates. As time evolves, the domain wall moves and roughens, while the bulk, i.e., spins far away from the domain interface, keeps invariant. As shown in Fig. 1, the time evolution of the spin configuration is displayed with the black and whites squares, corresponding to $S_i = \pm 1$, respectively. Complicated spin structure are found nearby the domain interface, such as overhangs and islands at the time $t = 1\ 000$ MCS.

According to earlier literatures [1, 38, 49], there are many different ways to define the domain interface. In this paper, we adopt a simple and popular definition based on the magnetization. Denoting a spin at site (x, y) by $S_{xy}(t)$, a microscopic height function of the domain interface is introduced,

$$h(y,t) = \frac{L_x}{2}[m(y,t) + 1], \tag{3}$$

where $m(y,t)$ is the linear magnetization defined as

$$m(y,t) = \frac{1}{L_x}\left[\sum_{x=1}^{L_x} S_{xy}(t)\right], \tag{4}$$

and L_x is the size of the lattice in the x direction. The velocity of the domain interface is then calculated as

$$v(t) = \frac{d\langle h(y,t)\rangle}{dt}, \tag{5}$$

where $\langle\cdots\rangle$ includes both the statistical average over samples and in the y direction. To depict the roughening process of the domain interface, the roughness function $\omega(t)$ and correlation function $C(r,t)$ are measured with

$$\omega^{(2)}(t) = \left\langle h(y,t)^2\right\rangle - \langle h(y,t)\rangle^2, \tag{6}$$

and

$$C(r,t) = \langle h(y+r,t)h(y,t)\rangle - \langle h(y,t)\rangle^2, \tag{7}$$

respectively. The former describes the roughening of the domain interface in the x direction, and the latter reflects the growth of the spatial correlation in the y direction. Moreover, the function $F(t)$ is measured as the ratio of the planar susceptibility and line susceptibility [48, 49, 50],

$$F(t) \sim [M^{(2)}(t) - M(t)^2]/\omega^2(t), \tag{8}$$

where $M(t)$ is the total magnetization, and $M^{(2)}(t)$ is its second moment.

In addition, other types of the quenched disorder are also considered for comparison, taking the random-bond disorder in the DBDIM as an example. The Hamiltonian of the DBDIM is

$$\mathcal{H} = -\sum_{<ij>} J_{ij}S_iS_j - H\sum_i S_i, \tag{9}$$

where $J_{ij} = 1 + \varepsilon_{ij}$ denotes the nearest-neighboring coupling strength, and ε_{ij} is the bond disorder following a Gaussian distribution with the mean zero and the standard deviation σ. Without loss of generality, we set $\sigma = 1.5$ in the simulations as an example of the strong-disorder case.

2.2. Extended Monte Carlo (EMC) algorithm

In usual Monte Carlo simulations, we are limited to the system size $L_x = 2L_y = 2\ 048$ up to $t_{max} = 2\ 000$ MCS for a sufficiently large sample size $N_s = 20\ 000$ [48, 50], since all of the spins in the lattice, on average, should be chosen and updated in each MCS. However, the number of the activated spins $N(t)$ decreases quickly with the time t, as shown in Fig. 1. Where the activated spin is defined that each attempt of the flip will be accepted once the spin is chosen. As an example, $N(t) = 68$ is obtained at $t = 1\ 000$ MCS, much smaller

than the total spin number $2L^2 \approx 10^6$. Consequently, most of the spins are inactivated in Monte Carlo simulations. To avoid the undesirable waste of the time, the EMC algorithm is developed in this paper with the architecture:

Step 1: Initialize the spin lattice with a perfect domain interface. The quenched disorder $h_i(x, y)$ is generated randomly for each site in the rectangle lattice.

Step 2: Create a table list of the activated spins. To be specific, we search for the spins with the energy change $\delta E < 0$ according to Eq. (2), and store their position information (x, y) in the table list. The number of activated spins $N(t)$ is then obtained as the size of the table list.

Step 3: Update the table list. In this table list, we randomly choose a spin, flip it with $S_i \to -S_i$, and delete its position information. Afterwards, the change of the energy δE is respectively calculated for its four nearest-neighboring spins. If $\delta E < 0$, new position information is added into the table list.

Step 4: Increase the time of the EMC simulation to $t' = t + 1/N(t)$ MCS. Physical observable of the system including the microscopic height function $h(y, t')$, roughness function $\omega(t')$, and correlation function $C(r, t'))$, are then assessed.

Step 5: Repeat the steps 3 and 4 until the time of the simulation $t > t_{max}$ indicating that a sample of the simulation is terminated.

Step 6: Repeat the steps $1 \sim 5$ for the statistical average over samples and realizations of the quenched disorder. The velocity of the domain interface $v(t)$ is then calculated with Eq. (5).

With the EMC algorithm, the depinning transition with lattice sizes from $L = 32$ to 12 000 is investigated up to $t_{max} = 22\,000$ MCS. Our main results are presented at $L = 8\,192$, much larger than $L = 1\,024$ in earlier literatures [48, 50], and simulation results at $L = 12\,000$ confirm that finite-size effects are already negligibly small. Besides, the influence of the disorder strength is also investigated, taking the uniformly distributed random field h_i with the strength varying from $\Delta = 0$ to 10. For each set of the parameters, more than 20 000 samples are performed for average. Statistical errors are estimated by dividing the total samples in three subgroups. If the fluctuation in the time direction is comparable with or larger than the statistical error, it also will be taken into account.

2.3. Scaling analysis

As the depinning transition is of second order, the short-time scaling theory [52, 53] is applicative for the time evolution of the order parameter $v(t)$. The dynamic scaling form is derived by scaling arguments with a finite lattice size L and nonequilibrium spatial correlation length $\xi \sim t^{1/z}$,

$$v(t, \tau, L) = b^{-\beta/\nu} G(b^{-z} t, b^{1/\nu} \tau, b^{-1} L), \tag{10}$$

where b denotes an arbitrary rescaling factor, β and ν correspond to the static exponents, z is the dynamic exponent, and $\tau = (H - H_c)/H_c$. Setting $b \sim t^{1/z}$,

the scaling form can be simplified in the short-time scaling regime with $\xi(t) \sim t^{1/z} \ll L$,

$$v(t,\tau) = t^{-\beta/\nu z} G(t^{1/\nu z}\tau). \tag{11}$$

Only at the transition point $\tau = 0$, a power law behavior is expected,

$$v(t) \sim t^{-\beta/\nu z}. \tag{12}$$

The critical field H_c is then located by searching for the best power-law behavior of $v_{_M}(t,\tau)$. Afterwards, the critical exponent $\beta/\nu z$ is estimated from Eq. (12), and $1/\nu z$ is measured from the time derivative of $v(t,\tau)$ in Eq. (11),

$$\left.\frac{\partial \ln v(t,\tau)}{\partial \tau}\right|_{\tau=0} \sim t^{1/\nu z}. \tag{13}$$

The nonequilibrium correlation length $\xi(t)$ can also be extracted independently from the correlation function $C(r,t)$ defined in Eq. (7) with the scaling form

$$C(r,t) = \omega^2(t)\widetilde{C}\left(r/\xi(t)\right), \tag{14}$$

where $\widetilde{C}(s)$ is the scaling function with $s = r/\xi(t)$, and $\omega^2(t)$ is the roughness function defined in Eq. (6). With the correlation length $\xi(t)$ at hand, the roughness exponent ζ is estimated from the kinetic roughening of the domain interface,

$$\omega^2(t) \sim \left[\xi(t)\right]^{2\zeta}. \tag{15}$$

Meanwhile, one may determine the local roughness exponent ζ_{loc} by fitting $\widetilde{C}(r,t)$ with an empirical scaling form,

$$\widetilde{C}(r/\xi(t)) \sim \exp\left[-\left(r/\xi(t)\right)^{2\zeta_{loc}}\right]. \tag{16}$$

Though power law behaviors at the critical point are expected in Eqs. (12),(13) and (15) based on the scaling theory, corrections to scaling should be considered to extend the fitting to the early times. Usually, a power-law correction form is adopted,

$$y = ax^b(1 + c/x), \tag{17}$$

where the fitting parameter b corresponds to the critical exponent.

3. Numerical results

3.1. Superiority of the EMC algorithm

As it is referred above, the usual Monte Carlo method is time consuming to study the depinning phase transition in disordered media. To overcome it, an extensive version of the Monte Carlo method, i.e., EMC algorithm, has been introduced. In this subsection, we will compare the results obtained from the EMC with those obtained from the usual Monte Carlo method, including the CPU time and the velocity $v(t)$ of the domain interface.

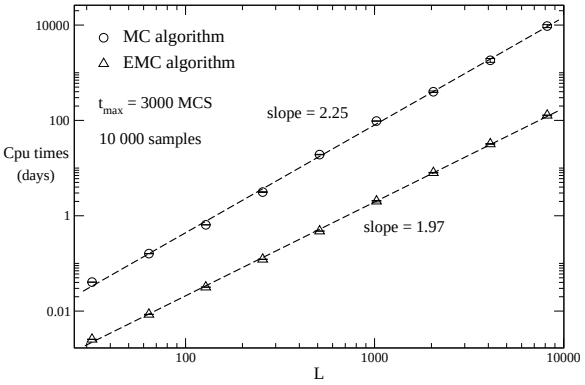

Figure 2: CPU time of the simulations based on the usual Monte Carlo algorithm (open circles) and EMC algorithm (open triangles) are displayed as a function of the lattice size L. The unit of the CPU time is one day. For each case of L, 10 000 statistical samples are performed for average, up to $t_{max} = 3000$ MCS, and error bars are also given. Dashed lines represent power-law fits.

In Fig. 2, the CPU time are shown for these two algorithms. For convenience of the comparison, we set the maximum value of the simulation time $t_{max} =$ 3 000 MCS and the size of the statistical samples $N_s = 10\ 000$. The open circles and open triangles correspond to the CPU time of the Monte Carlo (MC) and MEC algorithms, respectively, with one day as the unit. Generally speaking, the CPU time of the former is nearly 100 times larger than that of the latter, showing the great superiority of the EMC algorithm. As the lattice size L increases, a power-law behavior is observed for the CPU time, and the slope 1.97 of the EMC algorithm is a bit smaller than 2.25 of the usual Monte Carlo algorithm which means that the EMC algorithm is more efficient when the system size becomes larger, pointing to a possibility of the large-scale simulations for the depinning transition in DRFIM. Since the CPU time obeys $\delta t \sim L^2$, a linear time complexity, i.e., $O(n)$, is revealed for the EMC algorithm, further confirming that the algorithm is optimized.

Besides, the accuracy of EMC algorithm are also be carefully examined, in comparison with that of the usual Monte Carlo algorithm. As shown in Fig. 3, the velocity of the domain interface $v(t)$, as the order parameter of the depiinning transition, is displayed as a function of the time t for different lattice sizes L. The symbols represent numerical results obtained by the usual Monte Carlo method, and solid and dash-dotted lines correspond to those obtained by the EMC algorithm. A driving field $H = 1.2933$ is then used, which was reported as the transition point at the disorder strength $\Delta = 1.5$ [48, 50]. With the scaling form in Eq. (10), the dynamic behavior $v(t) \sim t^{-\beta/\nu z} f(t/L^z)$ is deduced at $\tau = 0$, and the finite-size effect described by $f(t/L^z)$ can be easily controlled, i.e., it rapidly approaches a constant as L increases.

Two distinguishable scaling regimes are found in numerical results, which are separated by a characteristic time scale $t_L \sim L^z$. When $t < t_L$, the symbols

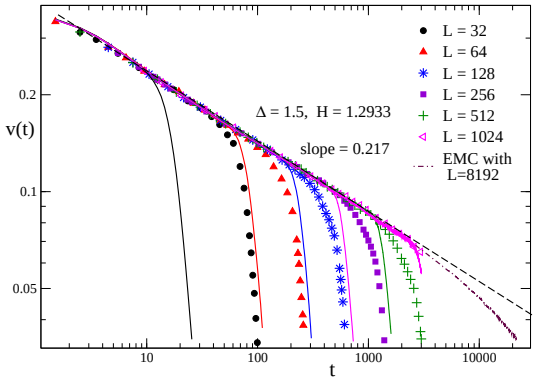

Figure 3: Velocity of the domain interface $v(t)$ defined in Eq. (5) is displayed for different lattice sizes L on a log-log scale. Other parameters, such as the driving field $H = 1.2933$ and disorder strength $\Delta = 1.5$, are used. The symbols represent the numerical results obtained by usual Monte Carlo method, and solid and dash-dotted line correspond to those obtained by EMC algorithm. Dashed line shows a power-law fit.

of different lattice size L nicely collapse to a master curve $v(t) \sim t^{-\beta/\nu z}$ with the slope 0.217(2), meaning an absence of the finite-size effect. The symbols are overlap with the corresponding solid lines, confirming that the numerical results obtained by these two algorithms are almost the same. Though the deviations of the symbols and lines are observed in the second time regime with $t > t_L$, one can use a sufficiently large lattice size, e.g., $L = 8192$, to make sure all the results in this paper staying in the first regime with $t_{max} < t_L$. Consequently, the EMC algorithm not only significantly saves the computing cost, but also has a high accuracy. Interestingly, the tail of the master curve, depicted by the dash-dotted line, exhibits a significant deviation from the power-law behavior marked by the dashed line, as shown in Fig. 3. It indicates that the driving field $H = 1.2933$ is smaller than the exact transition point H_c.

3.2. Depinning phase transition

Extensive numerical simulations are performed with the EMC algorithm to identify the depinning transition in disordered media. Unless otherwise stated, the lattice size $L = 8192$ is used in the following. Fig. 4 shows the dynamic relaxation of the number $N(t)$ of the activated spin under different driving fields H. Similar with the velocity $v(t)$ of the domain interface, the number $N(t)$ drops rapidly down for a small H, while approaches a constant for a large H. Searching for the best power-law behavior, one can locate the transition field $H_c = 1.29371(4)$, much more precise than the previous one 1.2933(2) obtained with the usual Monte Carlo method [48, 50]. In addition, another simulations with the lattice size $L' = 12\ 000$ are also carried out. Rescaled by a factor L'/L, the solid line, i.e., $N(t)$ at $L = 8192$, is in perfect agreement with the open circles and stars, corresponding to $N(t)$ and $v(t)L'$ at $L' = 12\ 000$, respectively, confirming that finite-size effect is already negligibly small. Moreover, an

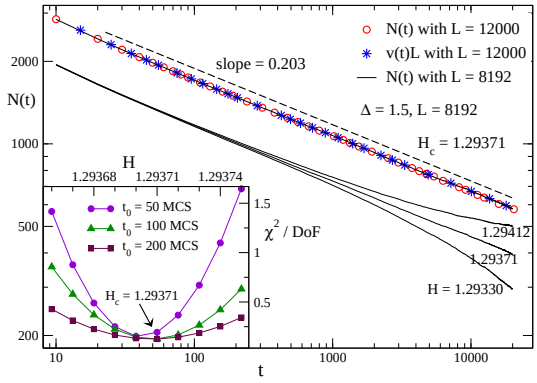

Figure 4: Dynamic relaxation of the activated-spin number $N(t)$ is plotted at $L = 8192$ for different driving fields H on a log-log scale. For clarity, the curve at the critical point $H_c = 1.29371$ is shifted up, in comparison with the number $N(t)$ of the activated spin and the velocity $v(t)L$ of the domain interface at $L = 12\ 000$. Dashed line shows a power-law fit. In the inset, the fitting error χ^2/DoF is shown for different waiting time $t_0 = 50, 100$, and 200 MCS.

almost-perfect power-law decay $N(t) = v(t)L \sim t^{\beta/\nu z}$ is observed at the transition point $H_c = 1.29371$. A direct measurement from the slope of the fitting yields $\beta/\nu z = 0.203(1)$.

To obtain a more accurate value of the transition point, the error of the power-law fitting χ^2/DoF [55] is carefully examined within a very narrow H-regime $[1.29366, 1.29375]$, as shown in the inset of Fig. 4. The critical point can be determined by judging the location of the minimization of χ^2/DoF. For different waiting time $t_0 = 50, 100$ and 200 MCS, an almost same value $H_c = 1.29371(1)$ is obtained, further showing that our result is robust and precise. In Fig. 5, the logarithmic derivatives of $N(t)$ and $v(t)$ in the neighborhood of $H_c = 1.29371$ are shown with open circles and stars, respectively. With the scaling form in Eq. (13), the exponent $1/\nu z = 0.677(3)$ is measured from the slope of the dashed line. To extend the fitting to earlier times of the numerical data, the correction to scaling is considered with the form in Eq. (17). The exponent $1/\nu z = 0.68(1)$ is then determined, consistent with the previous one within the error bar.

Besides the velocity of the domain interface, we also investigate the roughness function $\omega^2(t)$ and the correlation function $C(r, t)$ defined in Eqs. (6) and (7), respectively. With the scaling form of $C(r, t)$ in Eq. (14), numerical data at different time t collapse to the curve at $t' = 10\ 240$ MCS by rescaling r to $[\xi(t')/\xi(t)]r$ and C(r,t) to $[\omega^2(t')/\omega^2(t)]C(r, t)$. Adopting this data-collapse technique [56], one can extract the nonequilibrium correlation length $\xi(t)$ from the correlation function $C(r, t)$. The results are shown in Fig. 6 at the depinning field $H_c = 1.29371$ for the domain interface with $\Delta = 1.5$ (open circles) and the bulk with $\Delta = 0$ (open triangles). Power-law behaviors are observed for both of them with the slopes $1/z = 0.837(5)$ and $1/z_b = 0.663(5)$, respectively. However, an obvious deviation from the power law is found in the early times of the

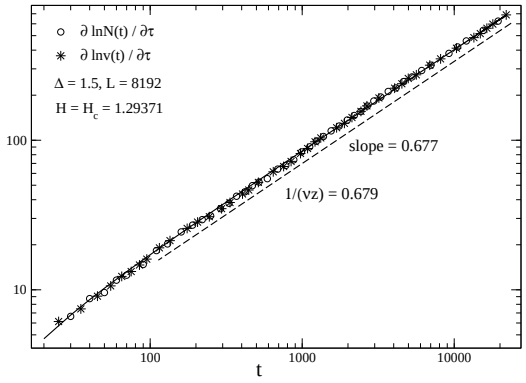

Figure 5: The logarithmic derivatives of $N(t)$ and $v(t)$ are displayed with open circles and stars, respectively, at the critical point $H_c = 1.29371$ for $\Delta = 1.5$ and $L = 8\ 192$. The dashed line represents a power-law fit, and the solid line shows a power-law fit with the correction defined in Eq. (17).

curve composed of open circles, thereby correction to scaling should be considered. With the correction form in Eq. (17), we refine the value of the exponent $1/z = 0.896(7)$. Moreover, a perfect coincidence between the open circles and pluses are observed, pointing to the relationship $F(t) \sim \xi(t)$, consistent with the prediction in earlier work [48]. In the inset, the scaling function $\widetilde{C}(r/\xi(t))$ is plotted as the function of r. Data of different time t nicely collapse to the curve at $t = 10\ 240$ MCS by rescaling r to $r/\xi(t)$, confirming the accurate of the correlation length. Moreover, the exponent $2\zeta_{loc} = 1.53(4)$ is measured by the fitting with Eq. (16).

With the correlation length $\xi(t)$ at hand, we then study the roughening process of the domain interface at the depinning transition. In Fig. 6, $\omega^2(t)$ is plotted as a function of $\xi(t)$ on a log-log scale. Obviously, $\omega^2(t)$ at the transition field $H_c = 1.29371$ with $\Delta = 1.5$ shows a cleaner power-law behavior than $\xi(t)$ does, and the roughness exponent $2\zeta = 2.00(2)$ is measured based on Eq. (15). It is much larger than $2\zeta_b = 0.97(1)$ for the bulk with $\Delta = 0$. In the inset, the roughness function $\omega(t)$ is displayed with the solid line, and the direct measurement of the slope yields $2\zeta/z = 1.65(2)$.

Finally, we summarize all the measurements of the critical exponents in Table. 1. The transition field $H_c = 1.29371(1)$ is more precise than the earlier result 1.2933(2) [48, 50], and significant deviations (reaching nearly $10\% \sim 30\%$) are also observed in the exponents ν, z, and ζ, showing the necessity of large-scale simulations for the depinining. For comparison, the exponents of the QEW equation [28, 34] are also shown in the table with the same lattice size $L = 8\ 192$. The contention that the depinnning transition of the DRFIM and QEW equation are not in a same universality class is supported by the distinct differences of the exponents between these two models, especially in β, z, and ζ. According to the arguments in Refs.[48, 49], the difference is mainly due to the overhangs and islands created in the depinning process of DRFIM.

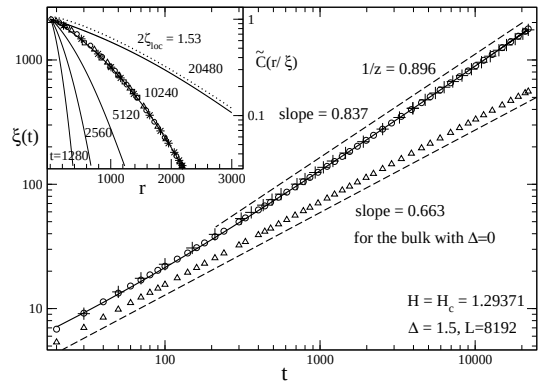

Figure 6: Time evolution of the nonequilibrium spatial correlation length $\xi(t)$ extracted from $C(r,t)$ is plotted for the domain interface with the disorder $\Delta = 1.5$ (open circles) and the bulk with $\Delta = 0$ (open triangles). Other parameters $H = 1.29371$ and $L = 8192$ are set. The pluses correspond to the function $F(t)$ defined in Eq. (8), dashed lines represent power-law fits, and solid line shows a power-law fit with the correction. In the inset, the scaling function $\widetilde{C}(r/\xi(t))$ is shown on a linear-log scale. Data collapse is demonstrated at $t = 10\ 240$ MCS, and the dotted line at $t = 20\ 480$ represents a fit with the form in Eq. (16).

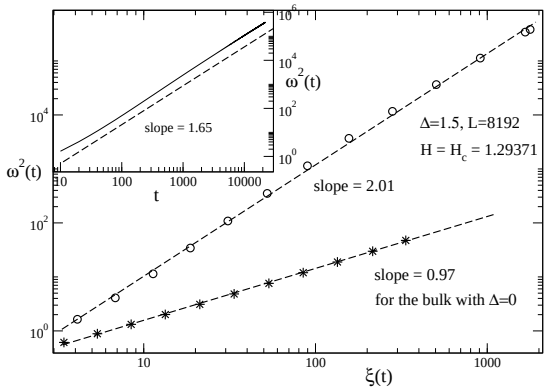

Figure 7: The roughness function $\omega^2(t)$ against the correlation length $\xi(t)$ is displayed with open circles and stars, corresponding to the cases with the disorder strengthes $\Delta = 1.5$ and 0, respectively. In the inset, time evolution of $\omega^2(t)$ is shown for $\Delta = 1.5$. Dashed lines represent power-law fits in Eq. (17).

Table 1: The transition point H_c and critical exponents for the depinning transition in DRFIM are obtained from the extensive simulations with the EMC algorithm, in comparison with those in the previous work and the QEW equation.

		QEW	DRFIM	
		Ref.[28, 34]	Previous work [48, 50]	This work
$v(t)$	H_c		1.2933(2)	1.29371(1)
	β	0.245(6)	0.295(3)	0.299(3)
	ν	1.333(7)	1.02(2)	1.32(2)
$\xi(t)$	z	1.433(6)	1.33(1)	1.12(1)
$\omega^2(t)$	ζ	1.250(5)	1.14(1)	1.00(1)
$C(r,t)$	ζ_{loc}		0.735(8)	0.76(2)
$H \gg H_c$	z_b		1.50(1)	1.51(1)
	ζ_b		0.49(1)	0.485(5)

3.3. New universality class

Does the depinning transition in the DRFIM belong to a universality class? To solve this issue, comprehensive simulations have been performed for different strengthes of the disorder (varying from $\Delta = 0$ to 10) in DRFIM and different types of the disorder, taking the random-bond disorder in the DBDIM as another example. As shown in Fig. 8, the phase boundary is displayed separating the depinning phase from the pinning phase. The vertical dash-dotted line indicates a critical value $\Delta_c = 1.0$ of the disorder, where the phase transition is of first order when $\Delta \leq \Delta_c$ and of second order when $\Delta > \Delta_c$. In both of them, linear behaviors are observed with the slopes 1.00 and 0.213(4), respectively. Unfortunately, the disorder strength $\Delta = 1.5$ which has been carefully investigated before is nearby the crossover between these two regimes, suggesting that the values of the exponents in Table. 1 may be Δ-dependent.

As an example, the velocity of the domain interface $v(t)$ at the critical point $\Delta_c = 1.0$ is shown in Fig. 9. Quite different from those in Figs. 3 and 4, $v(t)$ decays exponentially at $H \leq 0.99999$, and approaches a nonzero constant at $H \geq 1.00000$. A huge jump is then found in the steady-state velocity as the driving field is changed by only a paltry amount of 10^{-5}, inferring that it is a typical first-order phase transition, and the transition point is $H_c = 1.00000$. Similar phenomena are also found for the disorder strength $\Delta < \Delta_c$. While power-law decays of the domain interface are found at H_c for $\Delta > \Delta_c$, corresponding to the second-ordered phase transition. The critical exponents with respect to the disorder strength Δ are investigated carefully, and a scaling relation $\beta/\nu z + \zeta/z = 0.99(1)$ is revealed in Fig. 10 for sufficiently strong disorder, consistent with the prediction of the scaling theory $\beta = \nu(\zeta - z)$ in the QEW equation [36, 37]. It means that the roughness exponent ζ is not independent, and the roughening process of the domain interface $\omega^2(t) \sim t^{2\zeta/z}$ is merely induced by the depinning transition with $h(t) \sim t^{1-\beta/\nu z}$. In contrast, the other scaling relation $\nu = 1/(2-\zeta)$ is apparently violated, indicating the breaking down of the statistical tilt symmetry.

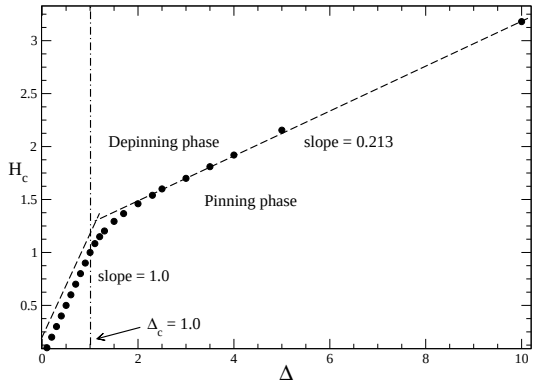

Figure 8: The phase boundary of the pinning-depinning transition H_c is plotted as a function of the disorder strength Δ. The vertical dash-dotted line indicates a critical disorder $\Delta_c = 1.0$, where the transition is of first order when $\Delta \leq \Delta_c$ and of second order when $\Delta > \Delta_c$. Dashed lines represent linear fits.

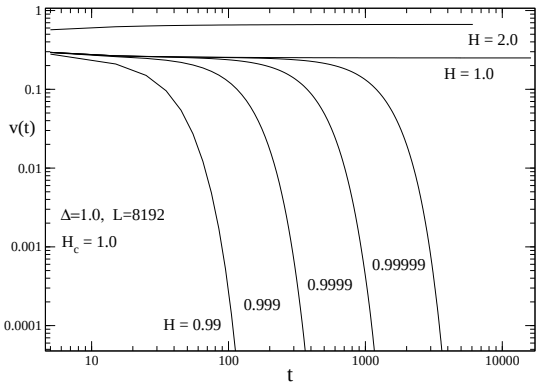

Figure 9: The velocity of the domain interface $v(t)$ is plotted at the critical value of the disorder $\Delta_c = 1.0$ for different driving fields H. The velocity $v(t)$ drops to zero quickly even at $H = 0.99999$, a slightly smaller than the transition point $H_c = 1.0$ where $v(t)$ approaches a nonzero constant.

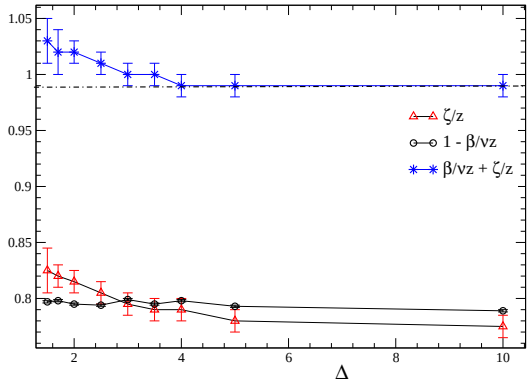

Figure 10: Variation of the critical exponents $1-\beta/\nu z$, ζ/z and $\beta/\nu z+\zeta/z$ are displayed as a function of the disorder strength Δ. The dash-dotted line points to an asymptotic value $\beta/\nu z+\zeta/z=0.99(1)$ in the regime of the strong disorder.

In addition, the robustness of the exponents ζ/z and $1-\beta/\nu z$ is affirmed in Fig. 10 for a wide window $\Delta\in[0,10]$, indicating a universality class. Furthermore, we summary the values of the exponents $\beta,\nu,z,\zeta,\zeta_{loc}$, and $\beta/\nu z+\zeta/z$ in Table. 2 for two cases with the disorder strengthes $\Delta=5.0$ and 10.0, respectively. For each exponent, a perfect consistency between these two cases is found within the error bars. In the same way, the depinning transition in the DBDIM is also investigated with a Gaussian distribution of the random-bond disorder. The standard deviation $\sigma=1.5$ is used in the simulations, which is already sufficiently large for the depinning transition. The results of these critical exponents listed in Table. 2 are almost the same with those obtained from the DRFIM with $\Delta=5.0$ and 10.0, but significantly differ from those of the QEW equation shown in Table. 1. It further supports our conclusion that the depinning transition in the Ising-type lattice models belong to a new universality class, though the scaling relation $\beta=\nu(z-\zeta)$ is still valid.

Table 2: The critical exponents of DRFIM and DBDIM are listed for the depinning transition in the strong-disorder regime. The values of these cases are consistent with each other, indicating a new universality class irrelevant to the disorder.

Disorder	β	ν	z	ζ	ζ_{loc}	$\beta/\nu z+\zeta/z$
DRFIM						
$\Delta=5$	0.304(5)	1.35(3)	1.12(1)	0.90(1)	0.67(1)	0.99(1)
$\Delta=10$	0.301(5)	1.29(3)	1.12(1)	0.89(1)	0.64(1)	0.99(1)
DBDIM						
$\sigma=1.5$	0.306(5)	1.31(3)	1.14(1)	0.90(1)	0.65(1)	1.00(1)

4. Conlusion

The depinning transition in Ising-type lattice models have been systematically investigated with the extensive simulations based on the developed EMC algorithm. In comparison with the usual Monte Carlo method, the EMC algorithm shows great superiority in the efficiency of the simulations, i.e., only about a percent of the CPU time is needed. Taking the DRFIM with the disorder strength $\Delta = 1.5$ as an example, we determined the transition field and critical exponents based on the short-time scaling form. The accuracy of the results is significantly improved by large-scale simulations with the lattice size up to $L = 8\ 192$, compared to those in earlier literature obtained at $L = 1024$ [48, 50]. The phase diagram of the dpinning transition is then identified with a critical value of the disorder strength $\Delta_c = 1.0$, separating the first-order transition form the second-order one. In the strong-disorder regime, the robustness of the exponents is uncovered for different strengthes (varying from $\Delta = 0$ to 10) and different types of the disorder (random filed in the DRFIM and random bond in the DBDIM). The results $\beta = 0.304(5), \nu = 1.32(3), z = 1.12(1)$, and $\zeta = 0.90(1)$ are quite different from those in the universality class of the Edwards-Wilkinson equation, though the scaling relation $\beta = \nu(\zeta - z)$ remains. It indicates that the depinning transition in the Ising-type lattice models belongs to a new universality class, due to the intrinsic anomalous scaling and spatial multiscaling. Moreover, the local roughness exponent $\zeta_{loc} = 0.65(1)$ is then measured from the correlation function $C(r, t)$, comparable with the experimental results in the ultrathin Pt/Co/Pt films [1].

Acknowledgements: This work was supported in part by the National Natural Science Foundation of China under Grant Nos. 11205043 and 11304072, and the authors thank Lu Wang and Tianci Zhou from the Zhejiang Universality for the insightful discussion.

References

[1] S. Lemerle, J. Ferré, C. Chappert, V. Mathet, T. Giamarchi, P. L. Doussal, Domain wall creep in an ising ultrathin magnetic film, Phys. Rev. Lett. 80 (1998) 849. doi:10.1103/PhysRevLett.80.849.

[2] C. J. Bolech, A. Rosso, Universal statistics of the critical depinning force of elastic systems in random media, Phys. Rev. Lett. 93 (2004) 125701. doi:10.1103/PhysRevLett.93.125701.

[3] P. L. Doussal, K. J. Wiese, E. Raphael, R. Golestanian, Can nonlinear elasticity explain contact-line roughness at depinning?, Phys. Rev. Lett. 96 (2006) 015702. doi:10.1103/PhysRevLett.96.015702.

[4] A. B. Kolton, A. Rosso, T. Giamarchi, W. Krauth, Dynamics below the depinning threshold in disordered elastic systems, Phys. Rev. Lett. 97 (2006) 057001. doi:10.1103/PhysRevLett.97.057001.

[5] M. B. Luo, X. Hu, Depinning and creep motion in glass states of flux lines, Phys. Rev. Lett. 98 (2007) 267002. doi:10.1103/PhysRevLett.98.267002.

[6] B. Bakó, D. Weygand, M. Samaras, W. Hoffelner, M. Zaiser, Dislocation depinning transition in a dispersion-strengthened steel, Phys. Rev. B 78 (2008) 144104. doi:10.1103/PhysRevB.78.144104.

[7] M. Y. Im, L. Bocklage, P. Fischer, G. Meier, Direct observation of stochastic domain-wall depinning in magnetic nanowires, Phys. Rev. Lett. 102 (2009) 147204. doi:10.1103/PhysRevLett.102.147204.

[8] J. Gorchon, S. Bustingorry, J. Ferré, V. Jeudy, A. B. Kolton, T. Giamarchi, Pinning-dependent field-driven domain wall dynamics and thermal scaling in an ultrathin Pt/Co/Pt magnetic film, Phys. Rev. Lett. 113 (2014) 027205. doi:10.1103/PhysRevLett.113.027205.

[9] M. Rost, L. Laurson, M. Dubé, M. Alava, Fluctuations in fluid invasion into disordered media, Phys. Rev. Lett. 98 (2007) 054502. doi:10.1103/PhysRevLett.98.054502.

[10] L. Du, H. Bodiguel, A. Colin, Thermally activated depinning motion of contact lines in pseudopartial wetting, Phys. Rev. E 90 (2014) 012402. doi:10.1103/PhysRevE.90.012402.

[11] G. Blatter, M. V. Feigel'man, V. B. Geshkenbein, A. I. Larkin, V. M. Vinokur, Vortices in high-temperature superconductors, Rev. Mod. Phys. 66 (1994) 1125. doi:10.1103/RevModPhys.66.1125.

[12] S. Okuma1, A. Motohashi, Critical behavior associated with transient dynamics near the depinning transition, New J. Phys. 14 (2012) 123021. doi:10.1088/1367-2630/14/12/123021.

[13] S. Brazovskii, T. Nattermann, Pinning and sliding of driven elastic systems: from domain walls to charge density waves, Adv. Phys. 53 (2004) 177. doi:10.1080/00018730410001684197.

[14] M. LeBlanc, L. Angheluta, K. Dahmen, N. Goldenfeld, Universal fluctuations and extreme statistics of avalanches near the depinning transition, Phys. Rev. E 87 (2013) 022126. doi:10.1103/PhysRevE.87.022126.

[15] S. Atis, A. K. Dubey, D. Salin, L. Talon, P. L. Doussal, K. J. Wiese, Experimental evidence for three universality classes for reaction fronts in disordered flows, Phys. Rev. Lett. 114 (2015) 234502. doi:10.1103/PhysRevLett.114.234502.

[16] M. Ovaska, L. Laurson, M. J. Alava, Quenched pinning and collective dislocation dynamics, Sci. Rep. 5 (2015) 10580. doi:10.1038/srep10580.

[17] J. C. Lee, K. J. Kim, J. Ryu, K. W. Moon, S. J. Yun, G. H. Gim, K. S. Lee, K. H. Shin, H. W. Lee, S. B. Choe, Universality classes of magnetic domain wall motion, Phys. Rev. Lett. 107 (2011) 067201. doi:10.1103/PhysRevLett.107.067201.

[18] D. Bang, H. Awano, Domain wall motion in Tb/Co multilayer wires with a large domain wall depinning field, J. Appl. Phys. 115 (2014) 17D512. doi:10.1063/1.4868918.

[19] Y. J. Shin, B. C. Jeon, S. M. Yang, I. Hwang, M. R. Cho, D. Sando, S. R. Lee, J. G. Yoon, T. W. Noh, Suppression of creep-regime dynamics in epitaxial ferroelectric bifeo$_3$ films, Sci. Rep. 5 (2015) 10485. doi:10.1038/srep10485.

[20] A. J. Ramsay, P. E. Roy, J. A. Haigh, R. M. Otxoa, A. C. Irvine, T. Janda, R. P. Campion, B. L. Gallagher, J. Wunderlich, Optical spin-transfer-torque-driven domain-wall motion in a ferromagnetic semiconductor, Phys. Rev. Lett. 114 (2015) 067202. doi:10.1103/PhysRevLett.114.067202.

[21] C. Wuth, L. Kolbe, G. Meier, Thermally activated stochastic domain-wall depinning in ferromagnetic nanowires, J. Appl. Phys. 114 (2013) 103901. doi:10.1063/1.4819808.

[22] V. O. Dolocan, Domain wall pinning and interaction in rough cylindrical nanowires, Appl. Phys. Lett. 105 (2014) 162401. doi:10.1063/1.4899128.

[23] S. Fukami, J. Ieda, H. Ohno, Thermal stability of a magnetic domain wall in nanowires, Phys. Rev. B 91 (2015) 235401. doi:10.1103/PhysRevB.91.235401.

[24] P. M. Shepley, A. W. Rushforth, M. Wang, G. Burnell, T. A. Moore, Modification of perpendicular magnetic anisotropy and domain wall velocity in Pt/Co/Pt by voltage-induced strain, Sci. Rep. 5 (2015) 7921. doi:10.1038/srep07921.

[25] M. Yamanouchi, J. Ieda, F. Matsukura, S. E. Barnes, S. Maekawa, H. Ohno, Universality classes for domain wall motion in the ferromagnetic semiconductor (ga,mn)as, Science 317 (2007) 1726. doi:10.1126/science.1145516.

[26] M. Hayashi, L. Thomas, R. Moriya, C. Rettner, S. S. P. Parkin, Current-controlled magnetic domain-wall nanowire shift register, Science 320 (2008) 209. doi:10.1126/science.1154587.

[27] S. S. P. Parkin, M. Hayashi, L. Thomas, Magnetic domain-wall racetrack memory, Science 320 (2008) 190. doi:10.1126/science.1145799.

[28] E. E. Ferrero, S. Bustingorry, A. B. Kolton, Nonsteady relaxation and critical exponents at the depinning transition, Phys. Rev. E 87 (2013) 032122. doi:10.1103/PhysRevE.87.032122.

[29] H. H. Boltz, J. Kierfeld, Depinning of stiff directed lines in random media, Phys. Rev. E 90 (2014) 012101. doi:10.1103/PhysRevE.90.012101.

[30] E. A. Jagla, Creep dynamics of viscoelastic interfaces, Europhys. Lett. 105 (2014) 46003. doi:10.1209/0295-5075/105/46003.

[31] Y. J. Chen, S. Zapperi, J. P. Sethna, Crossover behavior in interface depinning, Phys. Rev. E 92 (2015) 022146. doi:10.1103/PhysRevE.92.022146.

[32] J. M. López, M. A. Rodríguez, Interface dynamics at the depinning transition, J. Phys. I France 7 (1997) 1191. doi:10.1051/jp1:1997116.

[33] A. B. Kolton, A. Rosso, E. V. Albano, T. Giamarchi, Short-time relaxation of a driven elastic string in a random medium, Phys. Rev. B 74 (2006) 140201(R). doi:10.1103/PhysRevB.74.140201.

[34] J. M. Kim, H. Choi, Depinning transition of the quenched edwards-wilkinson equation, J. Korean Phys. Soc. 48 (2006) S241.

[35] O. Duemmer, W. Krauth, Critical exponents of the driven elastic string in a disordered medium, Phys. Rev. E 71 (2005) 061601. doi:10.1103/PhysRevE.71.061601.

[36] T. Nattermann, S. Stepanow, L. Tang, H. Leschhorn, Dynamics of interface depinning in a disordered medium, J. Phys. II France 2 (1992) 1483. doi:10.1051/jp2:1992214.

[37] P. L. Doussal, K. J. Wiese, P. Chauve, Two-loop functional renormalization group theory of the depinning transition, Phys. Rev. B 66 (2002) 174201. doi:10.1103/PhysRevB.66.174201.

[38] M. Jost, J. Heimel, T. Kleinefeld, Domain-wall roughening in $co_{28}pt_{72}$ alloy films, Phys. Rev. B 57 (1998) 5316. doi:10.1103/PhysRevB.57.5316.

[39] P. J. Metaxas, J. P. Jamet, A. Mougin, M. Cormier, J. Ferré, V. Baltz, B. Rodmacq, B. Dieny, R. L. Stamps, Creep and flow regimes of magnetic domain-wall motion in ultrathin pt/co/pt films with perpendicular anisotropy, Phys. Rev. Lett. 99 (2007) 217208. doi:10.1103/PhysRevLett.99.217208.

[40] M. Eltschka, M. Wötzel, J. Rhensius, S. Krzyk, U. Nowak, M. Kläui, T. Kasama, R. E. D. Borkowski, L. J. Heyderman, H. J. van Driel, R. A. Duine, Nonadiabatic spin torque investigated using thermally activated magnetic domainwall dynamics, Phys. Rev. Lett. 105 (2010) 056601. doi:10.1103/PhysRevLett.105.056601.

[41] A. Goussev, J. M. Robbins, V. Slastikov, Domain-wall motion in ferromagnetic nanowires driven by arbitrary time-dependent fields: An exact result, Phys. Rev. Lett. 104 (2010) 147202. doi:10.1103/PhysRevLett.104.147202.

[42] T. Gerhardt, A. Drews1, G. Meier, Current-driven domain wall depinning from an anisotropy boundary in nanowires, J. Phys.: Condens. Matter 26 (2014) 206001. doi:10.1088/0953-8984/26/20/206001.

[43] U. Nowak, K. D. Usadel, Influence of temperature on the depinning transition of driven interfaces, Europhys. Lett. 44 (1998) 634. doi:10.1209/epl/i1998-00519-4.

[44] F. Colaiori, G. Durin, S. Zapperi, Loss separation for dynamic hysteresis in ferromagnetic thin films, Phys. Rev. Lett. 97 (2006) 257203. doi:10.1103/PhysRevLett.97.257203.

[45] B. Koiller, M. O. Robbins, Growth and morphology transitions in anisotropic disordered media, Phys. Rev. B 82 (2010) 064202. doi:10.1103/PhysRevB.82.064202.

[46] B. Xi, M.-B. Luo, V. M. Vinokur, X. Hu, Depinning transition of a domain wall in ferromagnetic films, Sci. Rep. 5 (2015) 14062. doi:10.1038/srep14062.

[47] L. A. N. Amaral, A. L. Barabási, H. A. Makse, H. E. Stanley, Scaling properties of driven interfaces in disordered media, Phys. Rev. E 52 (1995) 4087. doi:10.1103/PhysRevE.52.4087.

[48] N. J. Zhou, B. Zheng, Y. Y. He, Short-time domain-wall dynamics in the random-field ising model with a driving field, Phys. Rev. B 80 (2009) 134425. doi:10.1103/PhysRevB.80.134425.

[49] N. J. Zhou, B. Zheng, Dynamic effect of overhangs and islands at the depinning transition in two-dimensional magnets, Phys. Rev. E 82 (2010) 031139. doi:10.1103/PhysRevE.82.031139.

[50] X. P. Qin, B. Zheng, N. J. Zhou, Universality class of the depinning transition in the two-dimensional ising model with quenched disorder, J. Phys. A: Math. Theor. 45 (2012) 115001. doi:10.1088/1751-8113/45/11/115001.

[51] L. Roters, A. Hucht, S. Lübeck, U. Nowak, K. D. Usadel, Depinning transition and thermal fluctuations in the random-field ising model, Phys. Rev. E 60 (1999) 5202. doi:10.1103/PhysRevE.60.5202.

[52] B. Zheng, Monte carlo simulations of short-time critical dynamics, Int. J. Mod. Phys. B 12 (1998) 1419. doi:10.1142/S021797929800288X.

[53] H. J. Luo, L. Schülke, B. Zheng, Dynamic approach to the fully frustrated xy model, Phys. Rev. Lett. 81 (1998) 180. doi:10.1103/PhysRevLett.81.180.

[54] L. Roters, S. Lübeck, K. D. Usadel, Creep motion in a random-field ising model, Phys. Rev. E 63 (2001) 026113.

[55] C. Chatelain, B. Berche, W. Janke, P. E. Berche, Softening of first-order transition in three-dimensions by quenched disorder, Phys. Rev. E 64 (2001) 036120. doi:10.1103/PhysRevE.64.036120.

[56] N. J. Zhou, B. Zheng, Nonsteady dynamic properties of a domain wall for the creep state under an alternating driving field, Phys. Rev. E 90 (2014) 012104. doi:10.1103/PhysRevE.90.012104.